

PAPER • OPEN ACCESS

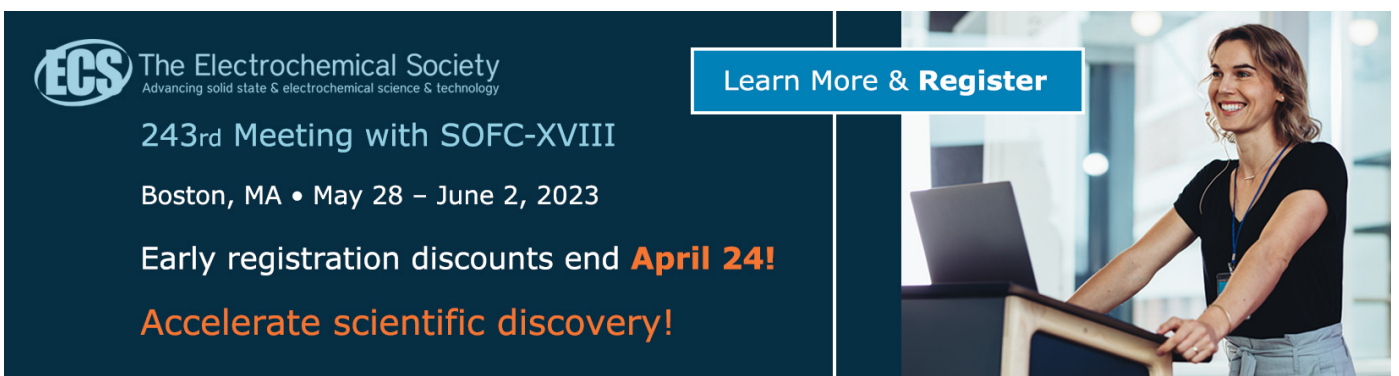
Computational modeling of confined blast waves with focus on interaction with structures

To cite this article: E Shehu *et al* 2023 *IOP Conf. Ser.: Mater. Sci. Eng.* **1275** 012028

View the [article online](#) for updates and enhancements.

You may also like

- [DYNAMICS AND AFTERGLOW LIGHT CURVES OF GAMMA-RAY BURST BLAST WAVES ENCOUNTERING A DENSITY BUMP OR VOID](#)
Z. Lucas Uhm and Bing Zhang
- [CHALLENGING SOME CONTEMPORARY VIEWS OF CORONAL MASS EJECTIONS. I. THE CASE FOR BLAST WAVES](#)
T. A. Howard and V. J. Pizzo
- [Blast Waves from Magnetar Flares and Fast Radio Bursts](#)
Andrei M. Beloborodov




ECS The Electrochemical Society
Advancing solid state & electrochemical science & technology

243rd Meeting with SOFC-XVIII
Boston, MA • May 28 – June 2, 2023

Early registration discounts end **April 24!**
Accelerate scientific discovery!

Learn More & Register



Computational modeling of confined blast waves with focus on interaction with structures

E Shehu, L Lomazzi, M Giglio and A Manes*

Politecnico di Milano, Department of Mechanical Engineering, Via La Masa n.1,
Milan 20156, Italy

*Email: andrea.manes@polimi.it

Abstract. Blast loading is a critical extreme loading condition for most engineering structures. Modeling such scenarios is challenging due to the intrinsic non-linearities. Recent numerical methods can capture the physics governing blast waves and their interaction with structures in a more accurate way than established empirical methods. This article is intended as a proof of concept that state-of-the-art CFD and FE software can be combined to set up high-fidelity uncoupled simulations. Computational fluid dynamics is exploited in this work to map the pressure field developed during a detonation reaction in a Eulerian domain. Then, such pressure time history is applied in the finite element framework to perform Lagrangian simulations. The methodology is used to compare the structural response of blast-loaded plates in fully confined environments to that in free-field scenarios. It turns out that confined blast waves are more severe than blast waves in unconfined scenarios, mainly due to the multiple reflections and residual quasi-static pressure. Moreover, on the one hand, the quasi-static pressure appears to contribute to further increasing the plate out-of-plane deflection, while on the other hand, it prevents plates from undergoing reverse buckling or oscillations around the initial equilibrium configuration. Experimental tests are required to provide further evidence about the latter contribution.

1. Introduction

The failure of safety-critical components in oil & gas or chemical plant facilities, bad handling of dangerous materials and terrorist attacks can cause blast waves. Such high-pressure waves represent critical loading conditions to most engineering structures. Thus, several methods have been developed and proposed in the literature to evaluate the response of blast loaded structures, with the purpose of increasing their blast resistance capability. Historically, empirical methods were developed, based on data from experimental tests, both to characterize the unconfined propagation of blast waves and to predict the permanent response of blast loaded structures [1][2][3][4]. To date, the most employed empirical model has been the model proposed by Kingery and Bulmash [5], which also laid the foundations of the CONWEP approach [6]. Although the latter approach is not valid for near-field explosions, it has been successfully implemented in many commercial finite element solvers, such as in Abaqus [7]. High fidelity numerical simulations have recently been employed to boost the performance of predictive tools in the field of blast protection engineering. Specifically, such methods have been proved to provide accurate predictions even in case complex environments and structures are considered.



For instance, the description of blast waves propagating in confined spaces has progressed thanks to numerical frameworks, even though the response of blast loaded structures in such complex loading conditions still has to be fully characterized and understood.

Hence, this work presents an uncoupled numerical framework to compare the response of blast loaded plates in confined scenarios to that of structures in unconfined conditions. A dedicated methodology is developed to this purpose using Abaqus, since the capabilities of built-in modules in commercial finite element (FE) solvers are strongly limited when dealing with blast loads. The pressure loading acting on the structure is mapped through computational fluid dynamics (CFD) simulations. The mapped pressure is then applied in a pure Lagrangian finite element (FE) simulation to characterize the transient structural response. Results of simulations in unconfined scenarios are compared to those obtained using the built-in CONWEP module in Abaqus to validate the proposed methodology.

This work is organized as follows. The Section *Methodology* introduces the framework used to simulate blast loaded structures. The framework is then applied to describe a case study in Section *Case study*, and results are described in Section *Results*. Conclusions are drawn out from this work in the Section *Conclusions*.

2. Methodology

Over the last decades, the constantly increasing computational power led to fast development and employment of software packages to numerically simulate scenarios described by the interaction of blast waves and deformable structures. To date, the uncoupled Eulerian Lagrangian (UEL) approach represents the most efficient numerical method in the blast protection engineering field, even though it cannot describe fluid-structure interaction (FSI) effects. According to the uncoupled scheme, the pressure field $p(x,y,t)$ describing the blast pressure exerted on the structure is obtained either by empirical models or by CFD simulations including the fluid domain only. Then, the pressure distribution along the fluid boundary is applied to the structure in a Lagrangian analysis. The procedure described above is schematically represented in Figure 1 and Figure 2.

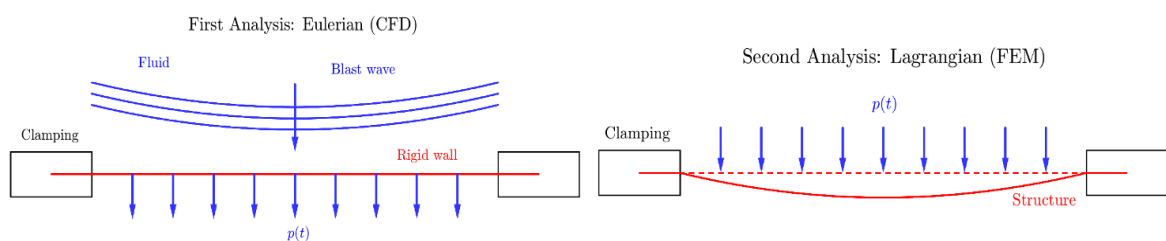


Figure 1. Uncoupled approach steps.

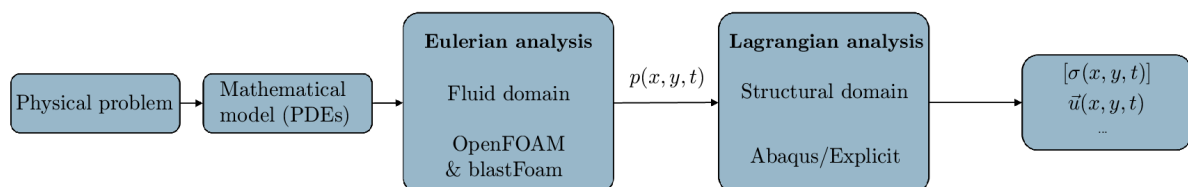


Figure 2. Required procedures to develop an Uncoupled Euler Lagrangian framework.

In this work, CFD simulations are performed in blastFoam [8], a new library dedicated to the computation of compressible flow with application to high-explosive detonation phenomena. Specifically, blastFoam is an entirely open-source toolbox based on OpenFOAM. The selected CFD

framework comes with several built-in equations of state for detonation dynamics and implements numerical explicit schemes dedicated to explosive phenomena. Using this CFD software package allows accurately mapping the load history exerted by blast waves on structures. That is, CFD simulations are used to overcome the strong limitations of built-in modules of commercial FE solvers, which fail to properly characterize blast wave loading in complex scenarios.

FE simulations are performed in Abaqus. This choice is mainly made because Abaqus allows implementing user Fortran subroutines to customize simulations. This makes it possible to define user-defined material models and to bridge CFD and FE analyses. Lagrangian simulations are carried out through the Abaqus\Explicit solver, due to the dynamic nature of the problem. Confined and unconfined blast waves are differentiated directly in the CFD environment by imposing proper boundary conditions for the fluid volume. As a result, two different pressure fields $p(x,y,t)$ are then applied as distributed loads in the FE simulations to the same steel plate.

3. Case study

Numerical simulations following the Uncoupled Eulerian Lagrangian scheme are set up to assess the effect of confinement on the structural response of steel plates. The same framework is applied to described both confined and unconfined blast events, which are differentiated through different boundary conditions. A spherical TNT charge is placed in the origin of a Cartesian reference frame centered in a cubic domain made of air (red sphere in Figure 3). In case of unconfined simulations, one rigid wall is modeled with a *slip* boundary condition, i.e., the component of velocity orthogonal to the wall is set to $v_y = \mathbf{v} \cdot \mathbf{j} = 0$ (grey faces in Figure 3). This assumption allows describing the reflection of blast waves. Other walls are set to *zeroGradient* boundary condition, that extrapolates field quantities to the patch from the nearest cell value, i.e., it allows the free propagation of blast wave out of the domain when boundaries are reached. Instead, in case of entirely confined analyses, all faces of the cube are assigned *slip* boundary conditions on the velocity component perpendicular to the wall. The symmetries of the problem are exploited to make numerical simulations run faster by modeling one eighth of the volume, as highlighted in orange in Figure 3.

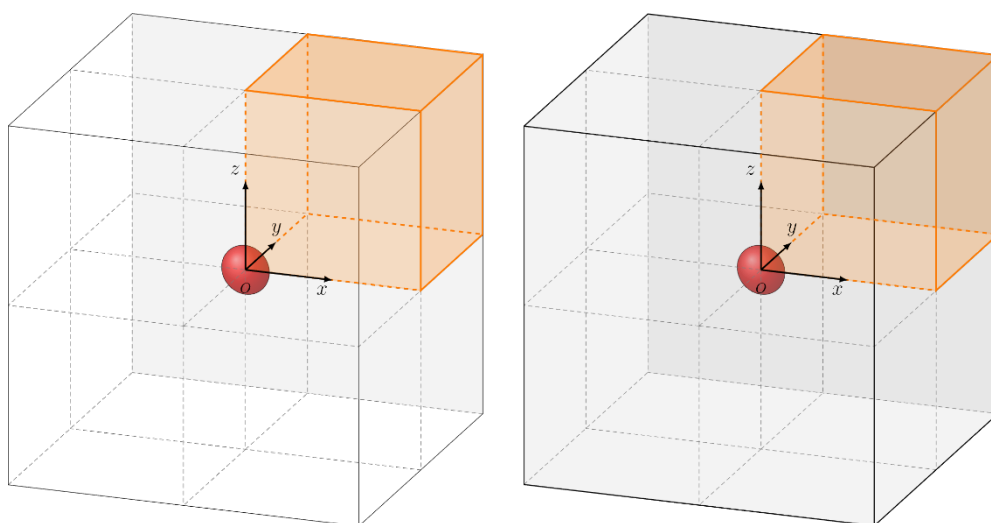


Figure 3. On the left the free-field blast case, on the right the fully confined blast case

The mathematical model employed to describe the detonation phenomenon of the explosive material is represented by the set of compressible Euler equations with reaction evolution [9]. Conservation of mass, momentum and energy equations are reported in Eq. 1

$$\begin{cases} \frac{\partial \rho}{\partial t} + \nabla(\rho \mathbf{u}) = 0 \\ \frac{\partial(\rho \mathbf{u})}{\partial t} + \nabla(\rho \mathbf{u} \otimes \mathbf{u} + p \mathbf{I}) = 0 \\ \frac{\partial(\rho E)}{\partial t} + \nabla((\rho E + p) \mathbf{u}) = 0 \end{cases} \quad (1)$$

Euler equations are not a complete set of partial differential equations. Indeed, there are six unknowns p , ρ , v_x , v_y , v_z and E , but only five equations. One additional relationship should be provided to close the system. Hence, an equation of state (EOS) is added for each phase present in the domain. In the simulations carried out in this work, two phases are present in the system: air and explosive.

Underacted energetic materials can be modelled with several relationships that describe the behavior of the material subjected to high pressure, before the occurrence of the detonation reaction. The third order Birch-Murnaghan equation [10] is adopted to model the explosive charge sphere as reported in Eq.2. Data for TNT explosive are retrieved from [8][10] and reported in Table 1.

$$p = p_{ref} + \frac{3K_0}{2K'_0} \left[\left(\frac{\rho}{\rho_0} \right)^{7/3} - \left(\frac{\rho}{\rho_0} \right)^{5/3} \right] \cdot \left\{ 1 + 0.75(K'_0 - 4) \left[\left(\frac{\rho}{\rho_0} \right)^{2/3} - 1 \right] \right\} \quad (2)$$

Table 1. Numerical coefficient of TNT for third order Birch-Murnaghan EOS [8][11].

	ρ_0 (kg/m ³)	K_0 (GPa)	K'_0 (-)	p_{ref} (kPa)	γ (-)
TNT	1630	9.6	6.6	101.325	0.35

Where K_0 is the bulk modulus of the TNT explosive, K'_0 is the derivative of the bulk modulus w.r.t pressure variable p and γ is the Gruneisen coefficient.

Instead, detonation products of energetic materials are modelled with the Jones-Wilkins-Lee (JWL) equation [11] reported in Eq. 3. Parameters for TNT are reported in Table 2[8][12].

$$p = A \left(1 - \frac{\omega}{R_1 V} \right) \exp(-R_1 V) + B \left(1 - \frac{\omega}{R_2 V} \right) \exp(-R_2 V) + \frac{e\omega}{V} \quad (3)$$

Table 2. Numerical coefficient of TNT for JWL EOS [8][12].

	ρ_0 (kg/m ³)	A (GPa)	B (GPa)	R_1 (-)	R_2 (-)	ω (-)	e (MJ/kg)
TNT	1630	371.21	3.231	4.15	0.95	0.30	4.294

Where A , B , R_1 , R_2 , ω are material constant obtained from experimental data and e is defined as the internal energy per unit mass.

Air is modelled as a perfect gas that fills the computational domain in all the volume except for the part where the explosive charge is located. Equation of state is reported in Eq.4.

$$p = (\gamma - 1)\rho e \quad (4)$$

Table 3. Numerical coefficient of air modelled as a perfect gas [8].

	ρ (kg/m ³)	γ (-)	e (MJ/kg)
Air	1.225	1.4	0.224

Parameter γ is the specific heat ratio in Eq. 4.

A blast wave is characterized by sharp pressure gradient caused by the travelling of the discontinuity. Thus, discretization in both time and space plays a crucial role for the accuracy of the numerical solution. Ideally, all numerical simulations should be mesh-independent to describe the nature of the modelled phenomenon. According to the mesh sensitivity analysis performed in [13], hexahedral finite volumes with characteristic length $L = 1.25$ mm are adopted in the CFD analyses. That is, the mesh size determined in [13] is used in this case study, since that value already guaranteed convergence in more severe scenarios.

Instead, in regions of the domain where no sharp discontinuities are present there is no need to keep such a refined mesh. Hence, to improve computational efficiency, an adaptive mesh refinement (AMR) technique is introduced in the framework. A *scaledDelta* technique is adopted [8]. When the *scaledDelta* difference between pressures of two adjacent cells is lower than 5%, then the two cells are merged into a single cell and fluxes are recomputed.

In order to further simplify the analysis and reduce the computational burden, a built-in mapping algorithm is exploited. Such algorithm allows simulating the first part of the detonation of the explosive in a 1D mesh and mapping the pressure field into a 3D mesh before any interactions that could break the spherical symmetry occur. A graphical representation of the mapping technique is reported in Figure 4.

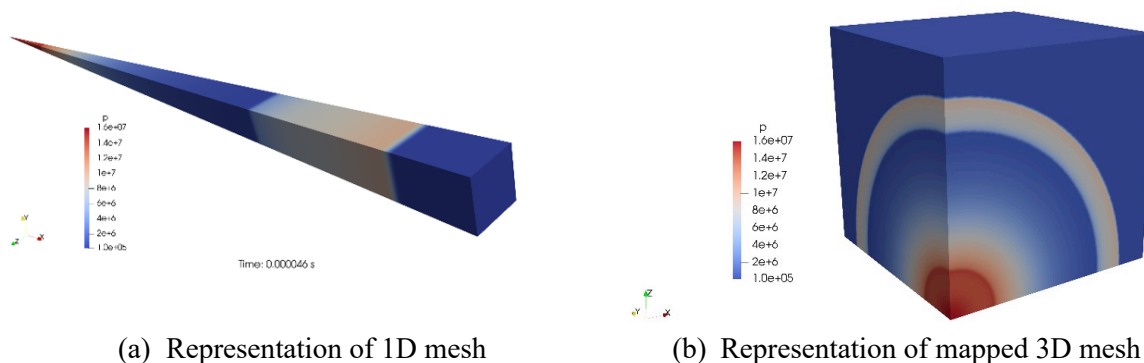


Figure 4. Graphical representation of the mapping technique.

A charge of 100 g of TNT at a stand-off distance of $L = 371$ mm is considered in the analyses. The length of the cube edge is set twice the stand-off distance to obtain a domain of the simulation with planar symmetries with respect to axes x , y and z . The choice of these parameters allows modeling one eighth of the volume as reported in Figure 3. Hence, the considered scaled distance is $Z = 0.4$ m/kg^{1/3}. Scaled distance is defined as the ratio between the stand-off distance and the cubic root of the explosive mass. According to this scaling law, blast phenomena and explosions characterized by the same scaled distance Z are described by the same properties.

A grid of virtual pressure gauges is located at the boundary wall where slip condition is applied. The pressure histories recorded from the pressure gauge located at (0, L, 0) in the unconfined and in the confined simulations are reported in Figure 5 and Figure 6, respectively.

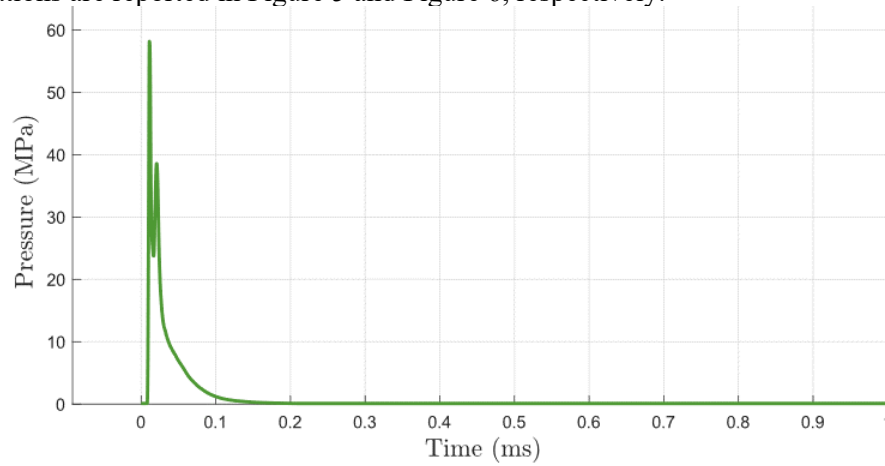


Figure 5. Unconfined blast at $Z = 0.4 \text{ m/kg}^{1/3}$

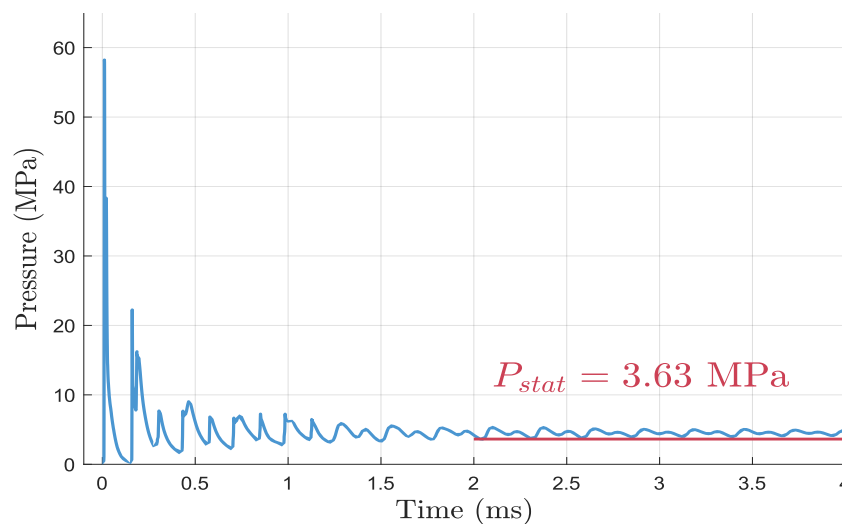


Figure 6. Fully confined blast at $Z = 0.4 \text{ m/kg}^{1/3}$

The two curves of Figures 5 and 6 have the same peak overpressure, but the confined case presents multiple peaks due to the reflections that occur in the closed domain. The quasi-static pressure in the confined scenario is also estimated by means of simple thermodynamic considerations. Approximating the air and detonation products to ideal gases, the quasi-static pressure inside the confined space is only influenced by the energy introduced by the detonation and is given by Eq. 5 [14]:

$$P_{stat} = \left(\frac{p_0}{\gamma_0 - 1} \cdot (V_{tot} - V_{expl}) + e_{expl} \rho_{expl} V_{expl} \right) \cdot \frac{\gamma - 1}{V_{tot}} \quad (5)$$

Where V_{tot} is the total volume of the cubic domain; V_{expl} is the volume of the explosive charge; γ and γ_0 are the specific heat ratio of detonation products and air respectively; p_0 is the ambient pressure; e_{expl} is the energy per unit volume of TNT and ρ_{expl} is the initial density of TNT.

Three different steel materials are considered to model the plates, thus resulting in three unconfined simulation and three confined simulations. The selected steels are DOCOL 600DL, DOCOL 1000DP and DOCOL 1400M produced by Swedish Steel AB (SSAB) [15]. Steel physical parameters are shared by the three alloys and are shown in Table 4. [16] [17].

Table 4. Physical parameters common for all steels.

	ρ_0 (kg/m ³)	E (MPa)	ν (-)
Steel	7850	210000	0.33

The modified Johnson Cook constitutive law, reported in Eq. 6, is employed to describe the material behavior under extreme loading conditions.

$$\sigma_y(\varepsilon_p, \dot{\varepsilon}_p, T) = \left(\sigma_0 + \sum_{i=1}^2 Q_i \cdot (1 - \exp(-C_i \cdot \varepsilon_p)) \right) \cdot \left(1 + \frac{\dot{\varepsilon}_p}{\dot{\varepsilon}_{p0}} \right)^c \cdot \left(1 - \left(\frac{T - T_r}{T_m - T_r} \right)^m \right) \quad (6)$$

The factor that considers the thermal contribution in Eq. 6 is not taken into consideration due to the adiabaticity of blast wave interaction. Once the elastic limit of the steel is reached, the material undergoes plasticization according to limit function reported in Eq.7.

$$f(\sigma_{ij}) = \Phi(\sigma_{ij}) - \sigma_y \quad (7)$$

Where Φ is the yield function according to Von Mises and σ_{ij} is the generic component of the stress tensor.

Table 5. Data for the three different steels used in the FEM simulations [17]

DOCOL	σ_0 (MPa)	Q_1 (MPa)	C_1 (-)	Q_2 (MPa)	C_2 (-)	c (-)	$\dot{\varepsilon}_{p0}$ (s ⁻¹)
600DL	325.7	234.8	56.2	445.7	4.7	0.010	0.0005
1000DP	468.8	517.1	185.2	258.3	12.3	0.008	0.0005
1400M	1114.8	341.8	1111.5	143.9	20.7	0.004	0.0005

A quarter of the plate is modelled exploiting symmetries. Fixed boundary conditions are applied along all edges of the plate. Shell elements S4R are used and shell thickness $t=2$ mm are chosen for all the plates, according to commercially available thicknesses for the selected materials. Time duration of the FE simulations is set to 4 ms considering the end of transient effect as reported in Figures 5 and 6. The acquired pressure field $p(x,y,t)$ is applied to a square plate with the same dimensions of a face of the Eulerian domain. The mesh size is equal to the spacing between virtual pressure gauges, so that each element in the FE simulation is assigned with the complete pressure history recorded by the corresponding probe in the CFD simulation. Thus, the mesh size of FE analyses is controlled by the number of probes in the CFD analyses. It was selected to set a 24x24 grid of evenly distanced pressure gauges over a quarter plate. Such value guarantees convergence of displacements and reduced FE simulation duration. Since no experimental data are available in the literature to validate the proposed methodology, the individual steps and their integration is validated through separate simulations. The convergence of CFD simulations is guaranteed by selecting the mesh size that was already identified in [13] for more sever case loading conditions. That mesh size was shown in [14] to accurately reproduce experimental observations. The link between the CFD and the FE solvers is validated by comparing the results in the uncoupled scenario with those generated through the built-in CONWEP module, which does not require passing data from external sources. Such a comparison is shown in Figure 7. Finally, the FE model includes material parameters already calibrated in other works, and the mesh size is selected through a convergence analysis, which is not reported here for the sake of brevity.

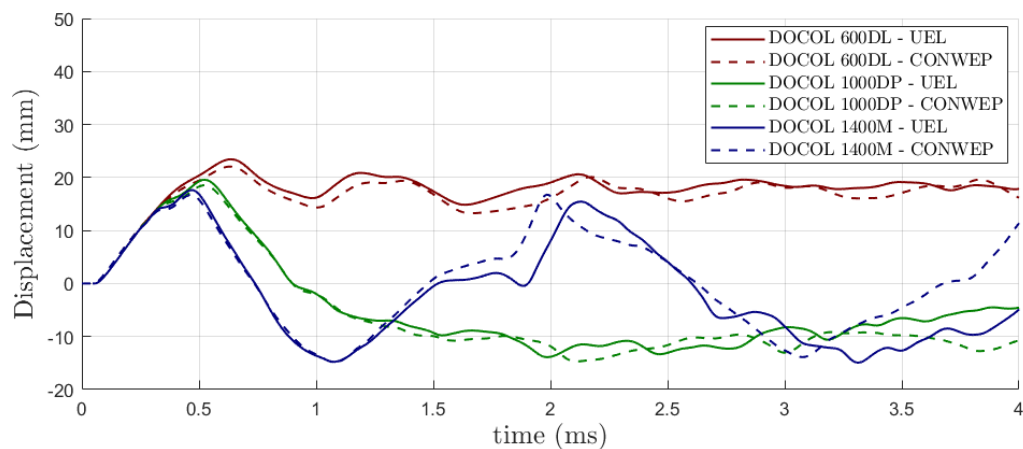


Figure 7. Comparison of midpoint displacement for different steels between CONWEP and UEL approaches.

4. Results

The results of the simulations with plates made of DOCOL 600DL, DOCOL 1000DP and DOCOL 1400M are reported in Figure 8, 9 and 10 respectively. Displacement time history of plates made of DOCOL 600DL, DOCOL 1000DP and DOCOL 1400M are reported in Figure 11, 12 and 13 respectively.

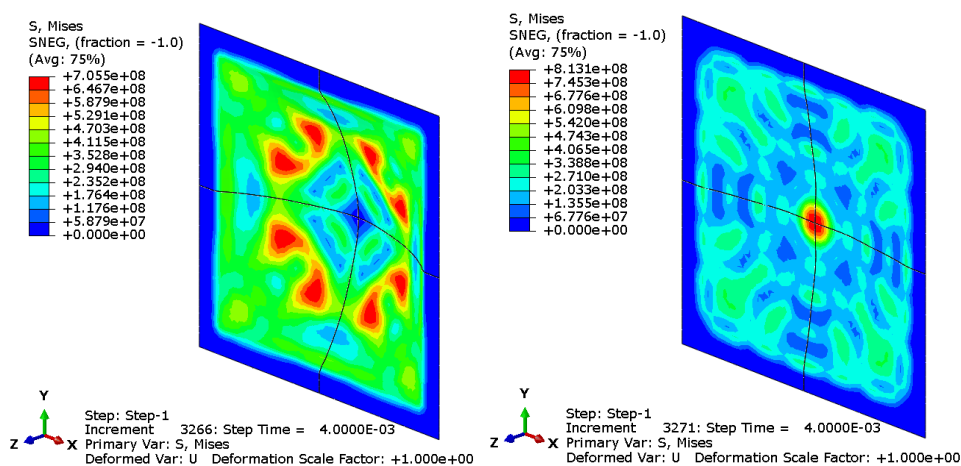


Figure 8. Von Mises stress field at the end of the simulation for the two plates made of DOCOL 600DL. Confined case (left) and unconfined case (right).

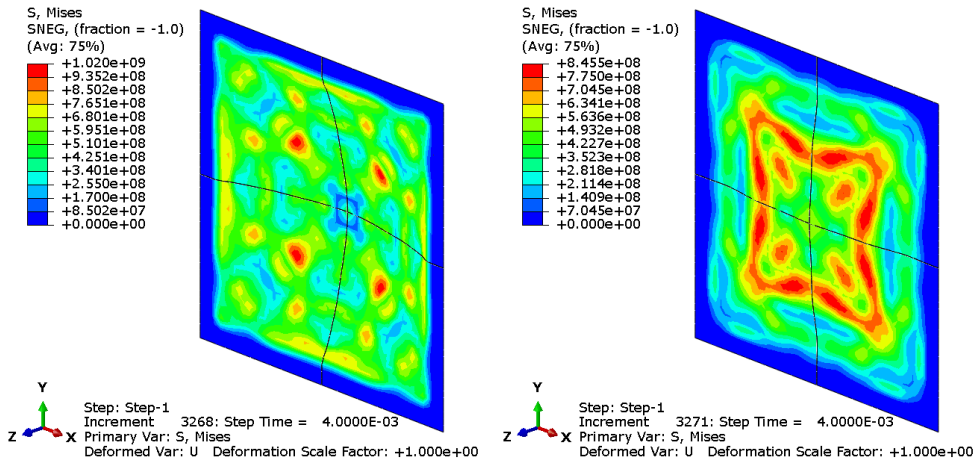


Figure 9. Von Mises stress field at the end of the simulation for the two plates made of DOCOL 1000DP. Confined case (left) and unconfined case (right).

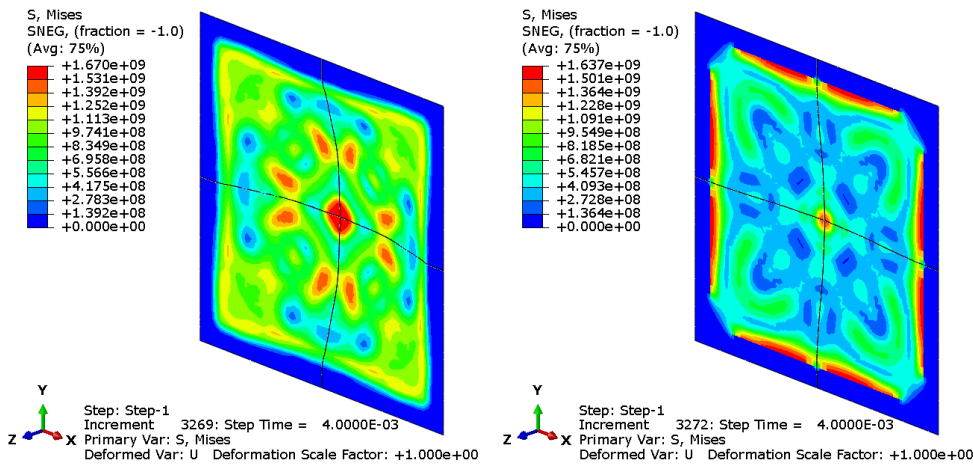


Figure 10. Von Mises stress field at the end of the simulation for the two plates made of DOCOL 1400M. Confined case (left) and unconfined case (right).

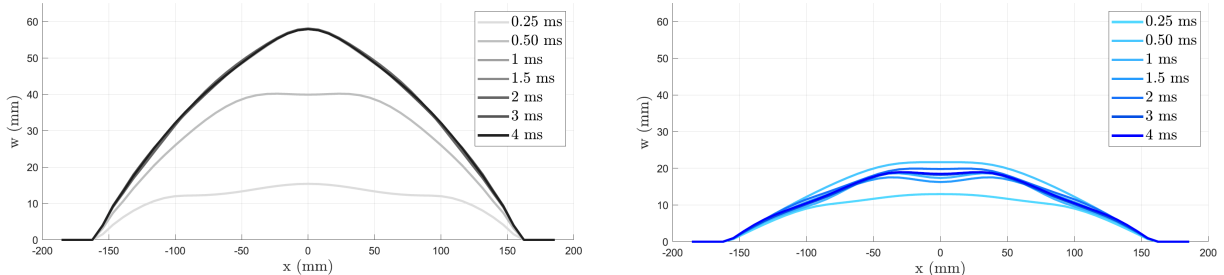


Figure 11. Displacement time history for DOCOL 600DL for the confined (left) and the unconfined (right) cases.

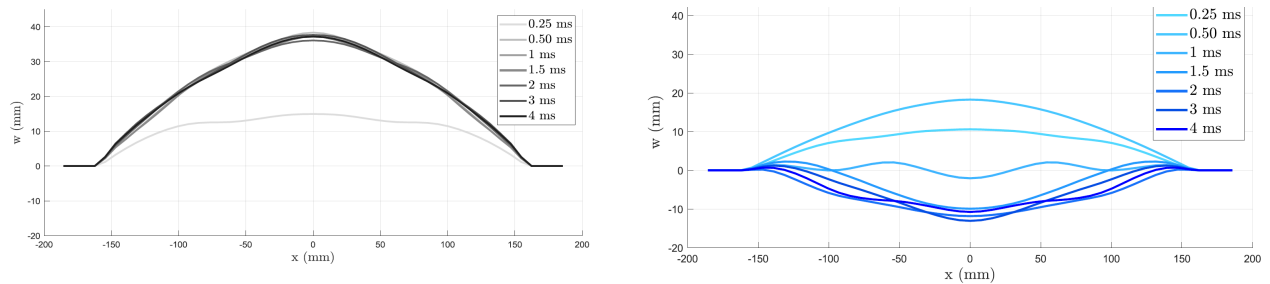


Figure 12. Displacement time history for DOCOL 1000DP for the confined (left) and the unconfined (right) cases.

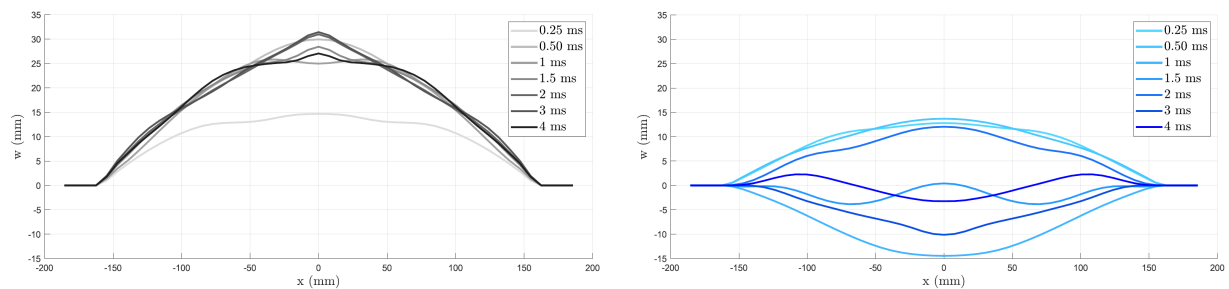


Figure 13. Displacement time history for DOCOL 1400M for the confined (left) and the unconfined (right) cases.

The most ductile of the three plates, DOCOL 600DL, experiences permanent plastic deformation in the direction of blast wave propagation in both confined and unconfined cases. What changes is the amount of displacement that is higher in the confined case. Compared to the free-field scenario, oscillations around the mean value are limited in the confined case.

The stiffest of the three plates, DOCOL 1400M, experiences the lowest permanent plastic deformation in the direction of blast wave propagation in the confined case. On the other hand, it behaves like an elastic membrane that oscillates around the equilibrium position in the unconfined case. However, plastic strain is present in the latter, as suggested by the high stress values. The overall behavior is similar to a plate that works in an elastic regime.

The behavior of the plate made of DOCOL 1000DP is unexpected. In fact, differently from what observed in the confined case in the unconfined scenario the plate shows a counter intuitive behavior, also known as reverse buckling [18], where the final permanent deflection of the plate is directed towards the blast-source.

Overall results for midpoint displacement are reported in Figure 14.

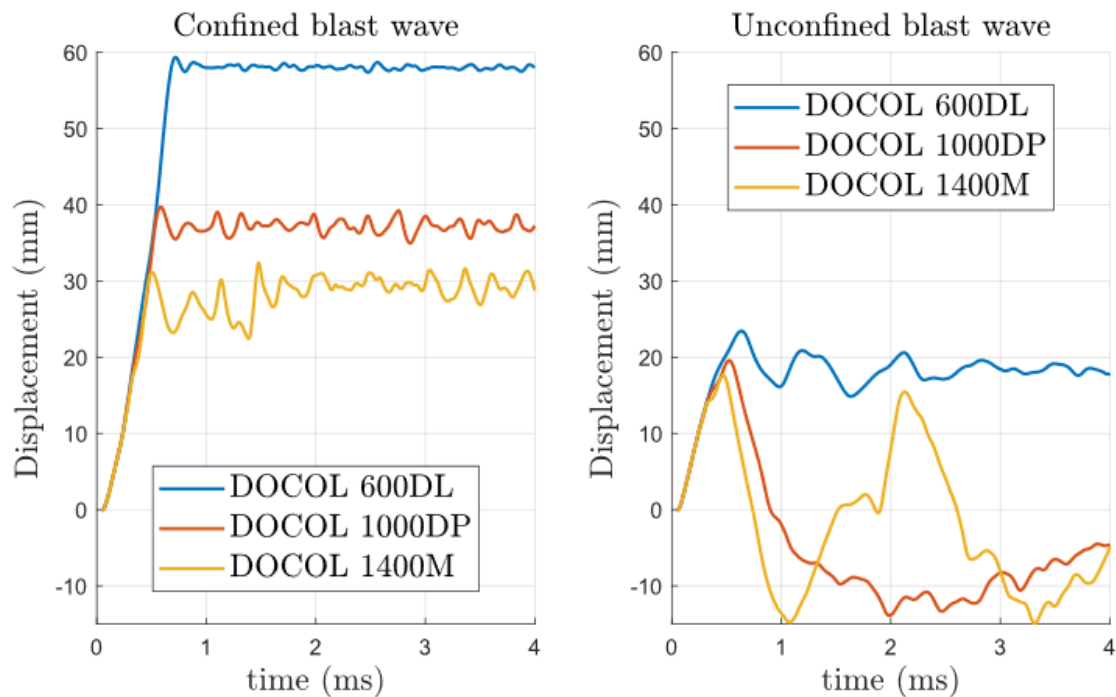


Figure 14. Representation of midpoint displacement for all the performed simulations.

5. Conclusions

In this work a high-fidelity numerical framework for uncoupled Eulerian-Lagrangian simulations of blast loaded plates is presented. The proposed approach is used to perform simulations of confined and unconfined blast scenarios. Results indicated that the presence of residual quasi-static pressure in confined blast events may prevent reverse buckling and oscillations around initial equilibrium configuration in steel plates. Moreover, plates made of different steels show different qualitative behaviors in unconfined cases: DOCOL 600DL undergoes plastic deformation, DOCOL 1000DP experiences reverse buckling and DOCOL 1400M vibrates as an elastic membrane.

Little is known in the literature about the main causes of reverse buckling, which is sometimes seen in case of short duration blasts and may be determined by the combination of inertia forces, elastic unloading forces and negative phase pressure of free-field blast waves. Note that the reverse buckling is not caused by geometric imperfections, which are not accounted for in this work. Moreover, the counter intuitive behavior is not influenced by curvature effects since the pressure loading is not influenced by the structural deformation in uncoupled simulations. In addition, von Mises stress values at final time of the simulations are considerably higher than yielding stresses σ_Y before the increase due to hardening. Consequently, the current approach may result to be insufficient for fully model the behavior of steel plates for the case $Z = 0.4 \text{ m/kg}^{1/3}$. A damage model capable of describing the perforation caused by ductile failure should be introduced to consider this possible event.

The introduction of a fracture model for the steel plate is expected to dramatically change the results for near-field explosions and it leads to the need for a new framework. This scenario highlights the limitation of Uncoupled Eulerian Lagrangian (UEL) approach because all considerations done in the current work rely on the presence of blast waves defined as distributed loads on each finite element of the plate. UEL simulations can be considered a fast and reliable numerical tool only when fracture does

not occur. Pressure leakage through the fractures generated in the plate can be modelled only by a fully Coupled Eulerian Lagrangian (CEL), where air is modelled on both sides of the plate.

Extensive numerical and experimental campaigns are required to characterize the behavior of steel plates subjected to blast loads. The authors suggest investigating in future works the influence of different parameters to understand which are the dominant variables that control the transition between different qualitative structural responses.

References

- [1] Nurick G N and Martin J B 1989 Deformation of thin plates subjected to impulsive loading—A review: Part I: Theoretical considerations *Int. J. Impact Eng.* **8** 159-170
- [2] Nurick G N and Martin J B 1989 Deformation of thin plates subjected to impulsive loading—A review part II: experimental studies *Int. J. Impact Eng.* **8** 171-186
- [3] Chung Kim Yuen S, Nurick G N, Langdon G S, Iyer Y 2017 Deformation of thin plates subjected to impulsive load: Part III – an update 25 years on *Int. J. Impact Eng.* **107**, 108-117
- [4] Lomazzi L, Giglio M and Manes A 2021 Analytical and empirical methods for the characterisation of the permanent transverse displacement of quadrangular metal plates subjected to blast load: Comparison of existing methods and development of a novel methodological approach *Int. J. Impact Eng.* **154**, 103890.
- [5] Kingery C N and Bulmash G 1984 *Air Blast Parameters from TNT Spherical Air Burst and Hemispherical Surface Burst* (Aberdeen Proving Ground, MD: U.S. Army Ballistic Research Laboratory)
- [6] Hyde D 1988 *Fundamentals of Protective Design for Conventional Weapons Microcomputer Programs CONWEP and FUNPRO, Applications of TM 5-855-1 (User's Guide)*. (Vicksburg, MS: Department of the Army, Waterways Experiment Station, Corps of Engineers)
- [7] Smith M 2009 *ABAQUS/Standard User's Manual*, Version 6.9.
- [8] Heylmun J, Vonk P and Brewer T 2021 *blastFoam 5.0 User Guide*, Synthetik Applied Technologies LLC
- [9] Stewart D S 1993 *Lectures on Detonation Physics: Introduction to the Theory of Detonation Shock Dynamics* (University of Illinois, Urbana, Illinois 61801)
- [10] Zheng Z and Zhao J 2016 Unreacted equation of states of typical energetic materials under static compression: A review *Chinese Physics B* **25** 076202
- [11] Lee E L, Hornig H C and Kury J W 1968 *Adiabatic expansion of high explosive detonation products* (Lawrence Radiation Laboratory Report UCRL-50422)
- [12] Dobratz B M 1985 *LLNL Explosives Handbook, properties of chemical explosives and explosive simulants* (Lawrence Livermore National Laboratory Report UCRL-51319)
- [13] Pannell J J, Panoutsos G, Cooke S B, Pope D J and Rigby S 2021 Predicting specific impulse distributions for spherical explosives in the extreme near field using a gaussian function *Int. J. Protective Structures*, **12**, 437–459
- [14] Feldgun V R, Karinski Y S and Yankelevsky D Z 2011 Some characteristics of an interior explosion within a room without venting *Structural Engineering and Mechanics* **38**, 633-649
- [15] <https://www.ssab.com/en/brands-and-products/docol> [Access: 2022-09-03]
- [16] Aune V 2017 *Behaviour and Modelling of Flexible Structures Subjected to Blast Loading* (Doctoral theses at NTNU 2017:101)
- [17] Aune V, Valsamos G, Casadei F, Langseth M and Børvik T 2017 On the dynamic response of blast-loaded steel plates with and without pre-formed holes *Int. J. Impact Eng.* **108**, 27-46
- [18] Nechitailo N 2013 *Reverse buckling and post-chaotic self-organization* (Amazon Kindle Direct Publishing 476)